DEVELOPMENT OF AN IMPROVED REPRESENTATION OF NEAR-FAULT GROUND MOTIONS

Paul Somerville

Woodward-Clyde, Pasadena, CA

ABSTRACT

The principal objective of this study is to develop an improved parameterization for the engineering specification of near-fault ground motions. In addition to the response spectrum, we would like to include time domain parameters that describe the near-fault pulse, such as its period, amplitude, and number of half-cycles. We have developed a preliminary model that relates time domain parameters of the near-fault ground motion pulse to the earthquake magnitude and distance. The model is for forward rupture directivity conditions, which produce a strong pulse of motion in the fault-normal direction. The pulse parameters that we have modeled are the period and peak amplitude of the largest cycle of motion of the velocity pulse. The records analyzed include 15 time histories recorded in the distance range of 0 to 10 km from earthquakes in the magnitude range of 6.2 to 7.3, augmented by 12 simulated time histories that span the distance range of 3 to 10 km and the magnitude range of 6.5 to 7.5.

INTRODUCTION

The objective of this study is to develop an improved representation of near-fault ground motions for use in building codes. The effects of rupture directivity on near-fault ground motions have been recognized by strong-motion seismologists for several decades. The propagation of fault rupture toward a site at a velocity close to the shear wave velocity causes most of the seismic energy from the rupture to arrive in a single large long-period pulse of motion that occurs at the beginning of the record (Somerville et al., 1997a). This pulse of motion, sometimes referred to as "fling," represents the cumulative effect of almost all of the seismic radiation from the fault. The radiation pattern of the shear dislocation on the fault causes this large pulse of motion to be oriented in the direction perpendicular to the fault, causing the strike-normal peak velocity to be larger than the strike-parallel peak velocity. Figure 1 shows these effects of rupture directivity in the time history of the Olive View recording of the 1994 Northridge earthquake.

Currently, all seismic design guidelines and codes specify design ground motions using the response spectrum. The effect of forward rupture directivity on the response spectrum is to increase the level of the response spectrum of the horizontal component normal to the fault strike at periods longer than 0.5 seconds (Somerville, 1996; Somerville et al., 1997a), as shown in Figure 2. This causes the peak response spectral acceleration of the strike-normal component to shift to longer periods, for example from 0.25 seconds to as much as 0.75 seconds. Near fault effects cannot be adequately described by uniform scaling of a fixed response spectral shape; instead the shape of the spectrum becomes richer in long periods as the level of the spectrum increases. A detailed model describing the amplitude and duration effects of rupture directivity

on near-fault ground motions was developed by Somerville et al. (1997a).

Current guideline and code documents that address near fault ground motions include SEAOC Vision 2000, the SEAOC Blue Book, the 1997 UBC, the 1997 NEHRP Seismic Provisions, and the FEMA-273 Rehabilitation Guidelines. These guideline and code documents recognize the importance of near-fault effect to varying degrees, but in most cases attempt to account for near-fault effects by increasing the design shear force. Two basic approaches are presently adopted. In the 1997 NEHRP provisions, mapped values of spectral ordinates at 1.0 second (obtained from the lesser of deterministic maps and probabilistic 2/50 maps) are used as the basis for determining the importance of near-fault effects. These mapped values are then multiplied by 2/3 to arrive at design spectral values from which the base shear is derived. In the 1997 UBC (and Appendix C of the 1996 SEAOC Blue Book), tables of near-source factors N_a and N_v are provided to amplify the design spectrum at distances less than 10 to 15 km from the seismic source. These near-source factors constitute the consensus of a SEAOC Seismology Subcommittee. Both approaches contain sound engineering judgment but result in somewhat different design values. Also, both approaches disregard the effect of pulse-like ground motions on the dynamic response of structures.

The quantification of the near-source factor in the SEAOC Blue Book and the 1997 UBC was based in part on the response spectral model developed by Somerville (1996) using strong motion recordings of the 1989 Loma Prieta, 1994 Northridge, and 1995 Kobe earthquakes. Specifically, the observations by Somerville (1996) concerning the dependence of the near-fault response spectral shape on magnitude and distance led to the incorporation of separate near-source factors for the acceleration and velocity parts of the response spectrum. As shown in Figure 2, the near-source spectrum in the 1997 UBC is compatible with the average of the two horizontal components of motion derived from the model of Somerville (1996) for both the design basis (10% in 50 years) and maximum capable (5% in 50 years) levels. However, the 1997 UBC does not specifically address the larger ground motion in the strike-normal component than in the strike-parallel component, which becomes especially significant for the maximum capable (5% in 50 years) level. The ground motion attenuation relations used in generating the NEHRP design values maps do not include any specific provision for the near-fault ground motion characteristics described above (Somerville et al., 1997a).

Although the response spectrum provides the basis for the specification of design ground motions in all current design guidelines and code provisions, there is a growing recognition that the response spectrum alone does not provide an adequate characterization of near-fault ground motions. For example, a broad consensus was reached at the NCEER Workshop on National Representation of Seismic Ground Motion for New and Existing Highway Facilities, held in San Francisco on May 29-30, 1997, that the response spectrum alone does not provide an appropriate characterization of near-fault ground motions for the design of bridges. This is because near fault ground motions are characterized by a relatively simple long period pulse of strong motion having relatively brief duration, rather than by a stochastic process having relatively long duration that characterizes more distant ground motion. Unlike the case for more distant ground motion, the resonance phenomenon that the response spectrum is designed to represent has insufficient time to build up when the input is a near-fault pulse. The response spectrum is thus not capable of adequately describing the seismic demands presented by a near-fault pulse.

The inadequacy of the response spectrum as a sole design criterion becomes readily apparent when time histories are selected to represent a design response spectrum. It is well known that a suite of different ground motion time histories which all match the same response spectrum produce variations in the response of a structure subjected to non-linear time history analysis. However, when the input time history is a near-fault pulse, this effect is accentuated to the point where small modifications of a near-fault time history that have no significant effect on the response spectrum can have a major effect on the response of a structure when subjected to non-linear time history analysis. This demonstrates that the current standard of practice does not provide a reliable basis for providing near-fault ground motion time histories that are specified solely on the basis of a design response spectrum.

Current trends in the development of future building codes have all embraced the concept of performance based design, and conceptual frameworks of that approach have been developed by SEAOC Vision 2000 and FEMA-273. Since the goal of performance based design depends heavily on realistic specification of ground motion inputs and realistic models of building response, it is clear that some alternative approach needs to be developed for specifying near-fault ground motions for seismic design. The new approach that we have developed has the goal of supplementing the response spectrum with time domain parameters such as the period and amplitude of the near-fault pulse. These ground motion parameters have been identified as being important for predicting damage to structures.

SELECTION OF NEAR-FAULT TIME HISTORIES

A set of near fault time histories was selected to systematically sample three variables: the magnitude range of 6.0 to 7.5, the distance range of 0 to 10 km, and directivity conditions ranging from forward to backward, in sets of both recorded and simulated time histories for soil conditions. Figure 3 displays the distribution of the selected soil time histories for magnitude vs. distance; directivity condition vs. magnitude, and directivity condition vs. distance for three sets: recorded data; simulations; and the combined recorded data and simulations.

Additional time histories for rock and soft soil conditions were included. However, except for the set of rock simulations, these do not systematically span the magnitude, distance and directivity condition ranges of interest. The recorded data set includes time histories from a variety of earthquake focal mechanisms, but does not systematically sample them, and the simulated time histories are all for strike-slip.

Tables 1 and 2 list the recorded and simulated time histories that were developed. Table 1 lists 29 recorded time histories. It includes all ten recorded time histories in the SAC Phase 2 near fault set (Somerville et al., 1997b), which were all for soil site conditions (either recorded on those conditions, or modified for those conditions). Ten soil site recordings have been added to produce a set of 20 time histories that span the magnitude range of 6.0 to 7.5, the distance range of 0 to 10 km, and a range of directivity conditions from forward to backward. Three soft soil recordings, and six rock recordings which also appear in the soil set after modification from rock to soil conditions, have also been added.

Table 2 lists 54 simulated time histories. It contains 27 time histories that were generated for rock conditions, and 27 time histories for soil conditions that were derived from the 27 simulations for rock. The 27 simulations span the magnitude range of 6.5 to 7.5, the distance range of 3 to 10 km, and a range of directivity conditions from forward to backward. The set of simulated time histories does not include those in the SAC Phase 2 Near Fault set, because they did not systematically sample the ranges of magnitude, distance and directivity condition. The time histories were generated using the procedure described by Somerville et al. (1996).

Forward directivity effects are manifested in the time histories as large velocity pulses on the strike normal component of ground motion, as shown in the Olive View recording of the 1994 Northridge earthquake (Figure 1). In Figure 4, the velocity response spectra of near fault recordings of three earthquakes show the dependence of the response spectral shape and level on earthquake magnitude and rupture directivity conditions. Forward rupture directivity effects are manifested in the response spectra by large long period ordinates on the strike-normal component.

IMPROVED PARAMETERIZATION OF NEAR-FAULT DESIGN GROUND MOTIONS

The principal objective of this study is to develop an improved parameterization for the engineering specification of near-fault ground motions. In addition to the response spectrum, the ground motion parameters include time domain parameters that describe the near-fault pulse, such as its period, amplitude, and number of half-cycles. Our goal is to select a set of parameters for representing near-fault ground motion that is optimally effective in predicting structural response.

We have developed a preliminary model that relates time domain parameters of the near-fault ground motion pulse to the earthquake magnitude. The model is for forward rupture directivity conditions, which produce a strong pulse of motion in the fault-normal direction. The pulse parameters that we have modeled are the period and amplitude of the largest cycle of motion of the velocity pulse. The records analyzed include 15 time histories recorded in the distance range of 0 to 10 km from earthquakes in the magnitude range of 6.2 to 7.3. Simple peak and trough representations of these time histories are shown in Figure 5 for comparison with the simple pulse models P1, P2 and P3 analyzed by Professor Krawinkler, as described later. These recorded pulses are augmented by 12 simulated time histories that span the distance range of 3 to 10 km and the magnitude range of 6.5 to 7.5, whose simple peak and trough representations are shown in Figure 6. All of the time histories are for soil site conditions, although in some cases rock time histories were spectrally modified to reproduce soil site conditions.

The preliminary relationship between the period T of the near-fault fault-normal forward directivity pulse recorded on soil and the moment magnitude M_w, assuming the period to be independent of distance, is:

$$\log10\ T = -2.5 + 0.425\ M_w$$

Constraining the relation between pulse period and magnitude to be self-similar, i.e. to

grow in proportion to the fault dimension, we obtain the relation shown in Figure 7:

$\log10\ T = -3.0 + 0.5\ M_w$

This relationship was also examined for separate sets of recorded and simulated time histories. It was found that the period of the recorded time histories grows more rapidly with magnitude than that of the simulated time histories. However, when the recorded and simulated time histories were combined, the resulting relationship was very similar to that of the recorded time histories.

An approximate relationship between the peak velocity PGV on soil of the near-fault fault-normal forward directivity pulse and the moment magnitude M_w and closest distance R is:

$\log10\ PGV = -1.0 + 0.5\ M_w - 0.5\ \log10\ R$

This model assumes a linear relationship between PGV and R which may not be realistic at very close distances; data recorded at distances of less than 3 km were not used in developing this relationship. This relationship was also examined for separate sets of recorded and simulated time histories. It was found that the peak velocity of the recorded time histories grows more rapidly with magnitude than for the simulated time histories, and decreases more gradually with distance than for simulated time histories. The approximate model given above is based on the recorded time histories and a subset of the simulated time histories that is most compatible with the recorded time histories. This subset consists of simulations for the magnitude range of 6.5 to 7.0 containing strong forward rupture directivity effects.

COMPARISON OF THE PULSE MODEL AND RECORDED PULSES WITH THE KRAWINKLER PULSE MODELS

The preliminary model of the pulse that we have developed addresses only the largest cycle of motion of the near-fault fault-normal forward directivity pulse. The model of the pulse is a symmetrical cycle of motion characterized by a peak, a trough and three zero crossings. To generate a more realistic time history from this simplified model, a continuous curve can be fit through these points using spline interpolation.

Our preliminary pulse model has one whole cycle of motion. Professor Krawinkler analyzed the response of structures to three different pulses, P1, P2 and P3, which are shown in Figure 6. These pulses have 0.5, 1 and 2.5 cycles of motion respectively. In our model, we have used the largest cycle of motion in the record, regardless of how many cycles it has, so our model is not quite the same as the P1 model of Professor Krawinkler.

In Table 3, we summarize how the 15 recorded pulses fit the three pulse models analyzed by Professor Krawinkler. Of the 15 near-fault pulses selected for analysis and provided to Professor Krawinkler, none provide a good fit to his P1 model, although 3 pulses are moderately well fit by that model. Of the 15 pulses, 9 fit his P2 model to the extent that the first peak and the following trough have larger peak velocity than the following peaks and troughs. Of these,

the first peak is larger in 6 and smaller in 3 than the following trough (the pulses are rectified so they all start upward with a peak). The remaining 6 time histories fit Professor Krawinkler's P3 model to the extent that subsequent peaks (or troughs) are larger than at least one of the first two peaks. In addition to these 6 time histories that fit P3, 5 of the 9 P2 pulses have subsequent peaks that are comparable to the first peak or trough, making a total of 11 time histories that are fit to some extent by the P3 model. This indicates the need to extend the preliminary pulse model presented here to include more half cycles, which in some cases come before the largest cycle (as in model P3) and in other cases come after.

RELATIONSHIP BETWEEN PULSE PERIOD AND RISE TIME

It is expected that the period of the pulse is most strongly influenced by the rise time T_R of slip on the fault, which measures the duration of slip at a single point on the fault. Somerville et al. (1998) found a self-similar relation between rise time and magnitude from an empirical analysis of 15 crustal earthquakes:

$$\log10\ T_R = -3.34 + 0.5\ M_w$$

The self-similar relation between pulse period and magnitude obtained above is:

$$\log10\ T = -3.0 + 0.5\ M_w$$

Eliminating M_w from these two equations, we find that the period T of the pulse is related to the rise time T_R by the relation:

$$T = 2.2\ T_R$$

The period of the pulse is thus equal to about twice the rise time of slip on the fault. This is consistent with the fact that the rise time is a lower bound on the period of the pulse. If the fault were a point source, then the only source parameter that would contribute to the period of the pulse would be the rise time, and the period of the pulse would equal the rise time if wave propagation effects such as Q are ignored. Since the fault is actually finite, and the rupture velocity is less than the shear wave velocity, the finite apparent duration of the rupture as observed at recording stations also contributes to the widening of the pulse, as described in the Appendix. For stations that experience forward rupture directivity, this apparent duration is much shorter than the actual duration of rupture.

DEPENDENCE OF RISE TIME (AND PULSE PERIOD) ON STYLE OF FAULTING

Analyses performed by Professor Krawinkler using pulse models P1, P2 and P3 demonstrate that the period of the near-fault pulse has a strong influence on the demands on the structure. We have just shown that the period of the pulse is directly related to the rise time. We have also found a correlation between rise time and faulting mechanism that may explain the style-of-faulting factor. For a given seismic moment, the rise times for reverse earthquakes are

on average about half as long as those for strike-slip earthquakes, as shown in Figure 8. Strong motion simulations show that halving the rise time causes an increase of about a factor of 1.4 in ground motion amplitudes. This increase is consistent with the style of faulting factor in empirical strong motion attenuation relations, in which ground motions for reverse earthquakes typically exceed those for strike-slip earthquakes by a factor ranging from about 1.3 to 1.4. Thus the larger ground motion levels in thrust faulting may be due to a shorter rise time. The shorter rise times of the reverse faulting events are manifested in the velocity response spectrum by a peak or plateau occurring at a shorter period than for strike-slip faults.

IMPORTANCE OF MULTIPLE PULSES

Structural response analyses by Professor Krawinkler using simple input pulses show that the response grows rapidly with the number of half-cycles of input motion. The presence of multiple pulses in the velocity time history can thus dramatically increase the damage potential of the ground motions. For example, the destructiveness of the ground motions from the 1995 Kobe earthquake was accentuated by the presence of two consecutive pulses in the recorded velocity waveforms, as shown in Figure 5. Some recordings of the 1994 Northridge and 1989 Loma Prieta earthquakes also contained velocity pulses having more than the 1 to 1½ cycles that characterize the simplest pulses recorded in other earthquakes. This indicates the need to identify the conditions that give rise to multiple pulses in near-fault ground motions. A preliminary review indicates that they may be due to multiple asperities on the fault rupture plane, and that their occurrence depends on the relative location of the hypocenter, of asperities on the fault, and of the recording site.

APPENDIX
CONTRIBUTION OF RISE TIME AND RUPTURE DURATION TO PULSE PERIOD

From the analysis of the data described above, we found that the period T of the pulse is related to the rise time T_R by the relation:

$$T = 2.2\ T_R$$

The period of the pulse is thus equal to about twice the rise time of slip on the fault. This is consistent with the fact that the rise time is a lower bound on the period of the pulse. In this appendix we use a simple analytical model to assess more quantitatively whether this relationship is compatible with fault rupture models. If the fault were a point source, then the only source parameter that would contribute to the period of the pulse would be the rise time, and the period of the pulse would equal the rise time if wave propagation effects such as Q are ignored. Since the fault is actually finite, and the rupture velocity is less than the shear wave velocity, the finite apparent duration of the rupture as observed at recording stations, defined to be the difference between the pulse duration and the rise time

$$t_a = T - T_R$$

also contributes to the widening of the pulse. From the relation between T and T_R given above,

$t_a = 1.2\ T_R$

For stations that experience forward rupture directivity, this apparent rupture duration is shorter than the actual duration of rupture, as shown in the analysis that follows.

The relation between fault rupture area A and magnitude for crustal earthquakes in tectonically active regions is given by (Somerville et al., 1998):

$\log10\ A = M_w - 3.95$

For a square fault of dimension L, this gives

$\log10\ L = 0.5\ M_w - 1.975$

The relation between rise time and magnitude from Somerville et al. (1998) is

$\log10\ T_R = 0.5\ M_w - 3.34$

Eliminating M_w, the relation between fault area A and rise time T_R is:

$\log10\ L = 1.365\ \log10\ T_R$

or fault dimension L in km = 23.2 x rise time T_R in seconds.

Somerville et al. (1997) analyzed ground motions recorded within 10 km of the fault. For forward rupture directivity, the fraction of the fault dimension that lies between the hypocenter and the recording site (parameter X for strike-slip, parameter Y for dip-slip) is 0.64, averaged over 44 recordings. The X and Y values are listed in Somerville et al. (1997), Table 8, and the identification of forward rupture directivity sites is listed in Somerville (1997), Table 1. Using the term F to represent the length of the fault between the hypocenter and the station, we then have

$F = 0.64\ L$ and hence

$F = 14.83\ T_R$

The time t for rupture to propagate across distance F, assuming a rupture velocity Vr of 2.75 km/sec (i.e. 0.8 times the shear wave velocity of 3.5 km/sec), is

$t = 5.4\ T_R$

The apparent duration t_a of the rupture across distance F as seen at a station is related to the actual duration t by the equation

$t_a = t\ (1 - (Vs/Vr)\ \cos\ \theta)$

where θ is the angle between the fault plane and the direction to the station. This relation strictly holds only at large distances from the fault where the angle θ is constant for all points on the fault. Somerville et al. (1997) analyzed ground motions recorded within 10 km of the fault. For forward rupture directivity, the angle between the fault plane and the recording site measured from the hypocenter (parameter θ for strike-slip, parameter ϕ for dip-slip) is 13 degrees, averaged over 44 recordings. The theta and phi values are listed in Somerville et al. (1997), Table 8, and the identification of forward rupture directivity sites is listed in Somerville (1997), Table 1. This gives

$t_a = 0.22\ t$

and

$t_a = 1.2\ T_R$

This relation between the apparent rupture time t_a and the rise time T_R, derived from a simple analytical model of fault rupture is the same as the result obtained above from analyzing the period of the pulse in the recorded data. Thus both the data and the simple analytical model indicate that the duration of the pulse T is related to the rise time T_R by the relation

$T = 2.2\ T_R$

REFERENCES

Somerville, P.G., K. Irikura, R. Graves, S. Sawada, D. Wald, N. Abrahamson, Y. Iwasaki, T. Kagawa, N. Smith and A. Kowada (1998). Characterizing earthquake slip models for the prediction of strong ground motion. *Seismological Research Letters*, submitted.

Somerville, P.G. (1997). Engineering characteristics of near fault ground motion, Proceedings, SMIP97 Seminar on Utilization of Strong Ground Motion Data, Los Angeles, May 8.

Somerville, P.G., N.F. Smith, R.W. Graves, and N.A. Abrahamson (1997a). Modification of empirical strong ground motion attenuation relations to include the amplitude and duration effects of rupture directivity, *Seismological Research Letters*.68, 180-203.

Somerville, P., N. Smith, S. Punyamurthula, and J. Sun (1997b). Development of ground motion time histories for Phase 2 of the FEMA/SAC Steel Project, Report No. SAC/BD-97-04

Somerville, P.G. (1996). Strong ground motions of the Kobe, Japan earthquake of Jan. 17, 1995, and development of a model of forward rupture directivity effects applicable in California, *Proceedings of the Western Regional Technical Seminar on Earthquake Engineering for Dams*, Association of State Dam Safety Officials, Sacramento, April 11-12.

Somerville, P., C.K. Saikia, D. Wald, and R. Graves (1996). Implications of the Northridge earthquake for strong ground motions from thrust faults, *Bull. Seism. Soc. Am.*, 86, S115-S125.

Table 1. Recorded Near-Fault Time Histories

Earthquake	Station	M	R	Directivity	Site	
Tabas	Tabas	7.4	1.2	backward	soil	
Landers	Lucerne	7.3	1.1	forward	mod to soil	rock
	Joshua Tree		7.4	backward	soil	
Mendocino	Petrolia	7.1	8.5	backward	soil	
Loma Prieta	LGPC	7.0	3.5	forward	mod to soil	rock
	Lexington		6.3	forward	mod to soil	rock
	Corralitos		3.4	backward	mod to soil	rock
Kobe	JMA	6.9	3.4	forward	mod to soil	rock
	Takatori		4.3	forward	soft soil	
	Port Island		6.6	forward	soft soil	
I.V. 1940	El Centro	6.9	10.0	backward	mod to soft soil*	
Northridge	Rinaldi	6.7	7.5	forward	soil	
	Olive View		6.4	forward	soil	
	Newhall		7.1	forward	soil	
	Sepulveda		8.9	forward	soil	
	Arleta		9.2	backward	soil	
Erzincan	Erzincan	6.7	2.0	forward	soil	
I.V. 1979	Array 5	6.5	4.1	forward	soil	
	Array 6		1.2	forward	soil	
	Bond's Corn		2.4	backward	soil	
Morgan Hill	Anderson D	6.2	4.5	forward	soil	
	Coyote L D		0.1	forward	mod to soil	rock
	Halls Valley		2.4	backward	soil	

* scaled to LA 10%in 50, then modified for soft soil response using SAC S1 model, 150 feet.

Table 2. Simulated Near-Fault Time Histories

Earthquake	Station	M	R	Directivity	Site	
7.5H4S2	4	7.5	3	backward	mod. to soil	rock
	6		3	forward	mod. to soil	rock
	8		3	forward	mod. to soil	rock
	4		5	backward	mod. to soil	rock
	6		5	forward	mod. to soil	rock
	8		5	forward	mod. to soil	rock
	4		10	backward	mod. to soil	rock
	6		10	forward	mod. to soil	rock
	8		10	forward	mod. to soil	rock
7.0H4S2	4	7.0	3	backward	mod. to soil	rock
	6		3	forward	mod. to soil	rock
	8		3	forward	mod. to soil	rock
	4		5	backward	mod. to soil	rock
	6		5	forward	mod. to soil	rock
	8		5	forward	mod. to soil	rock
	4		10	backward	mod. to soil	rock
	6		10	forward	mod. to soil	rock
	8		10	forward	mod. to soil	rock
6.5H4S2	4	6.5	3	backward	mod. to soil	rock
	6		3	forward	mod. to soil	rock
	8		3	forward	mod. to soil	rock
	4		5	backward	mod. to soil	rock
	6		5	forward	mod. to soil	rock
	8		5	forward	mod. to soil	rock
	4		10	backward	mod. to soil	rock
	6		10	forward	mod. to soil	rock
	8		10	forward	mod. to soil	rock

Table 3. Fit of 15 Recorded Near-Fault Pulses to the Krawinkler Pulse Models.

EARTHQUAKE	SITE	Fit to P1	Fit to P2	Fit to P3
Landers	Lucerne	x	x	
Loma Prieta	Los Gatos P. C.			x
	Lexington Dam		x	x
Kobe	JMA			x
	Takatori			x
	Port Island			x
Northridge	Sylmar		x	x
	Newhall			x
	Rinaldi	x	x	
	Sepulveda		x	x
Erzincan	Erzincan	x	x	
Imperial Valley '79	Array 6		x	
	Meloland		x	x
Morgan Hill	Anderson Dam			x
	Coyote Lake Dam		x	x

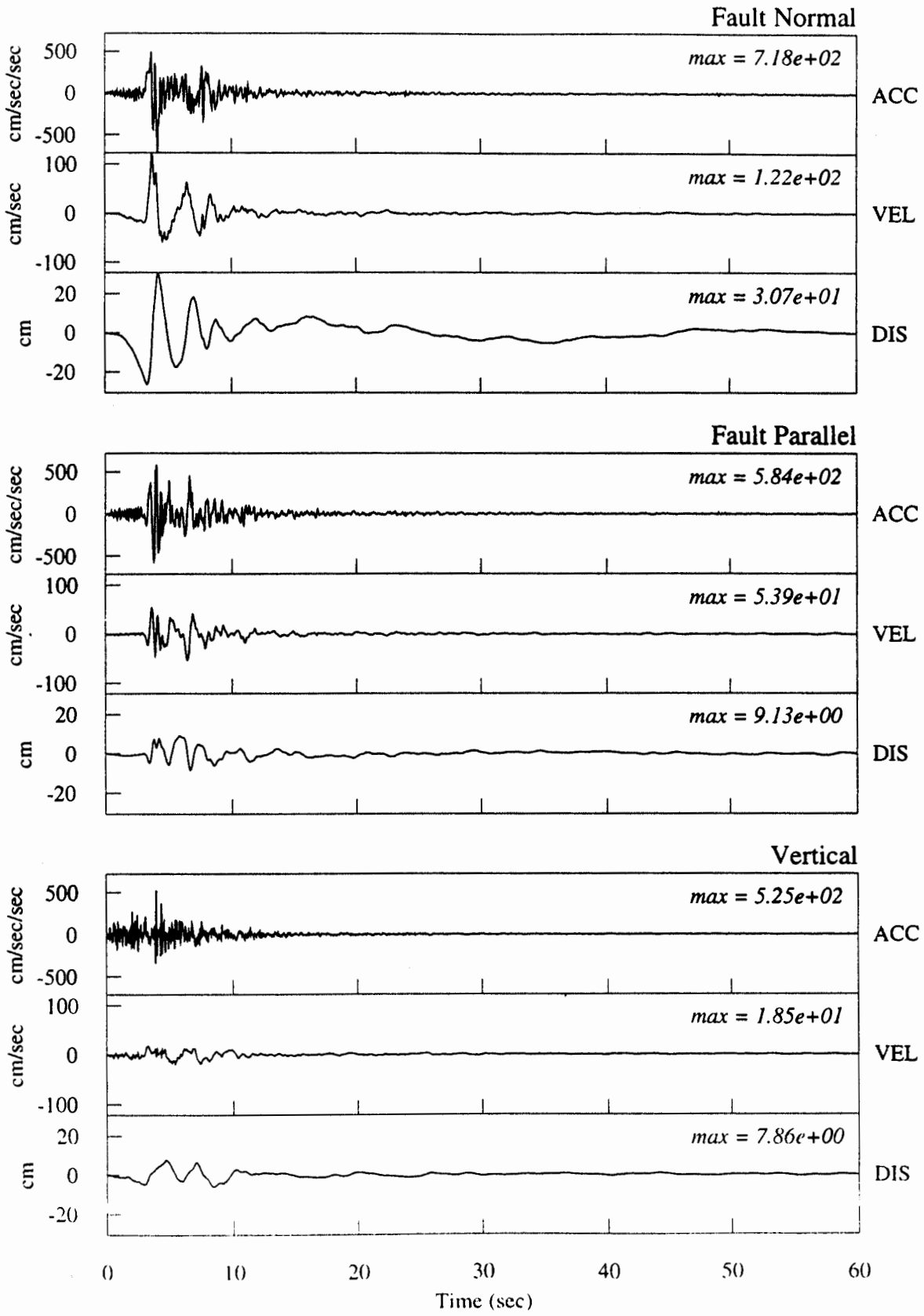

Figure 1. Olive View recording of the 1994 Northridge earthquake, containing a large velocity pulse.

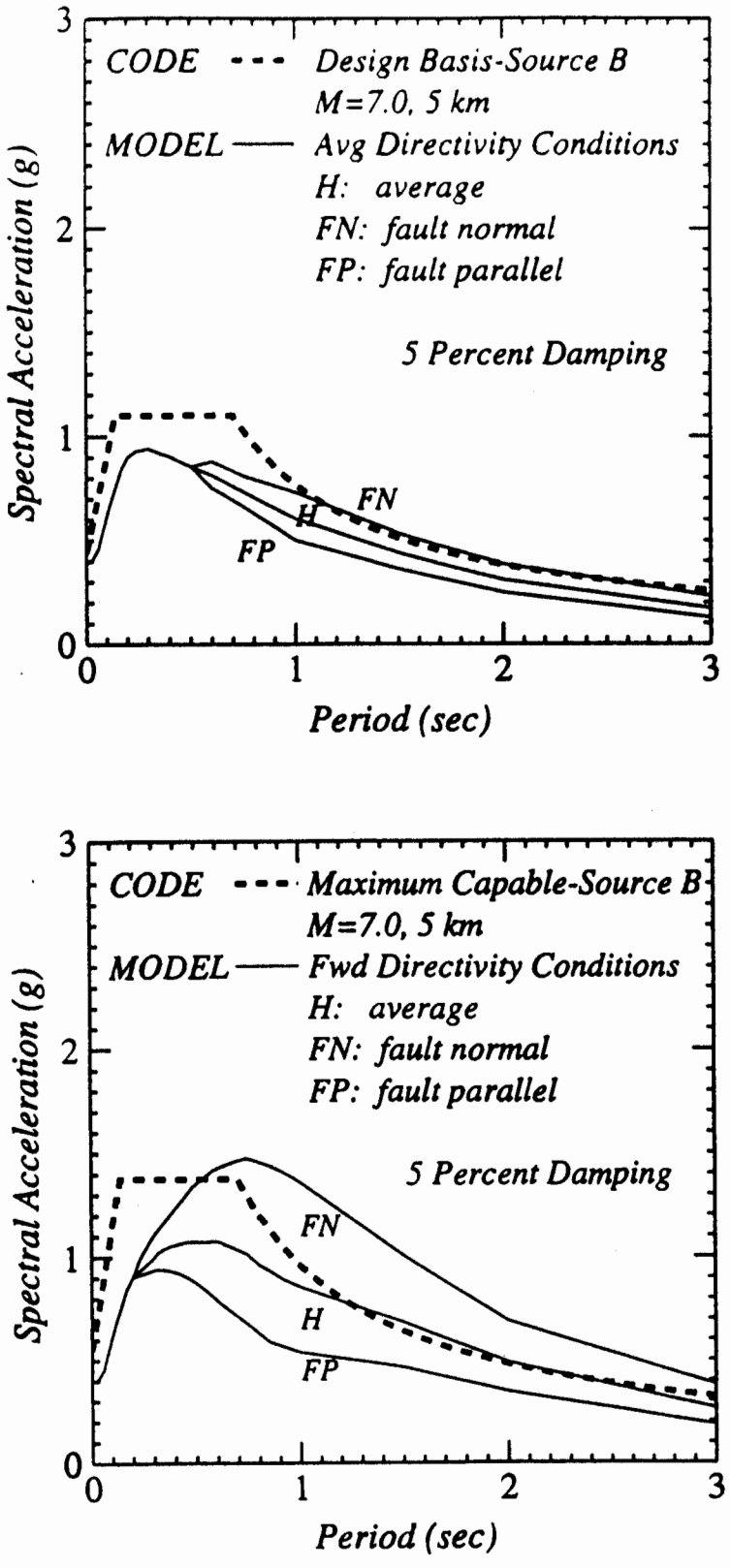

Figure 2. Response spectra for (top) average rupture directivity conditions and (bottom) forward rupture directivity conditions for a magnitude 7 earthquake at a distance of 5 km on soil. The response spectra are shown for the strike-normal, strike-parallel, and average horizontal components. Also shown for comparison are UBC spectra including the near-fault factor for design basis (top) and maximum capable (bottom) events.

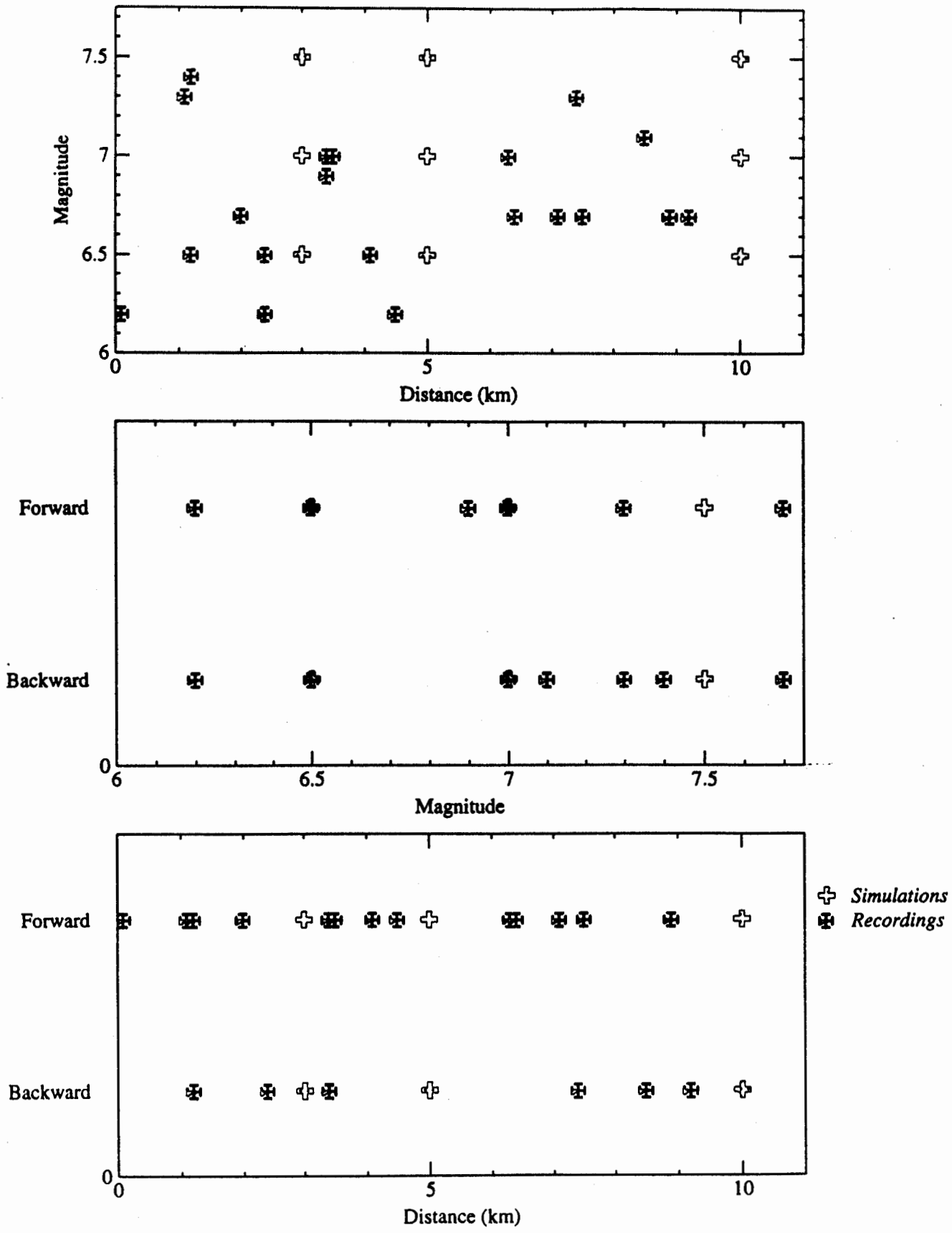

Figure 3. Distribution of recorded and simulated time histories. Top: magnitude vs distance; Center: directivity condition (forward or backward) vs. magnitude; Bottom: directivity condition (forward or backward) vs. distance.

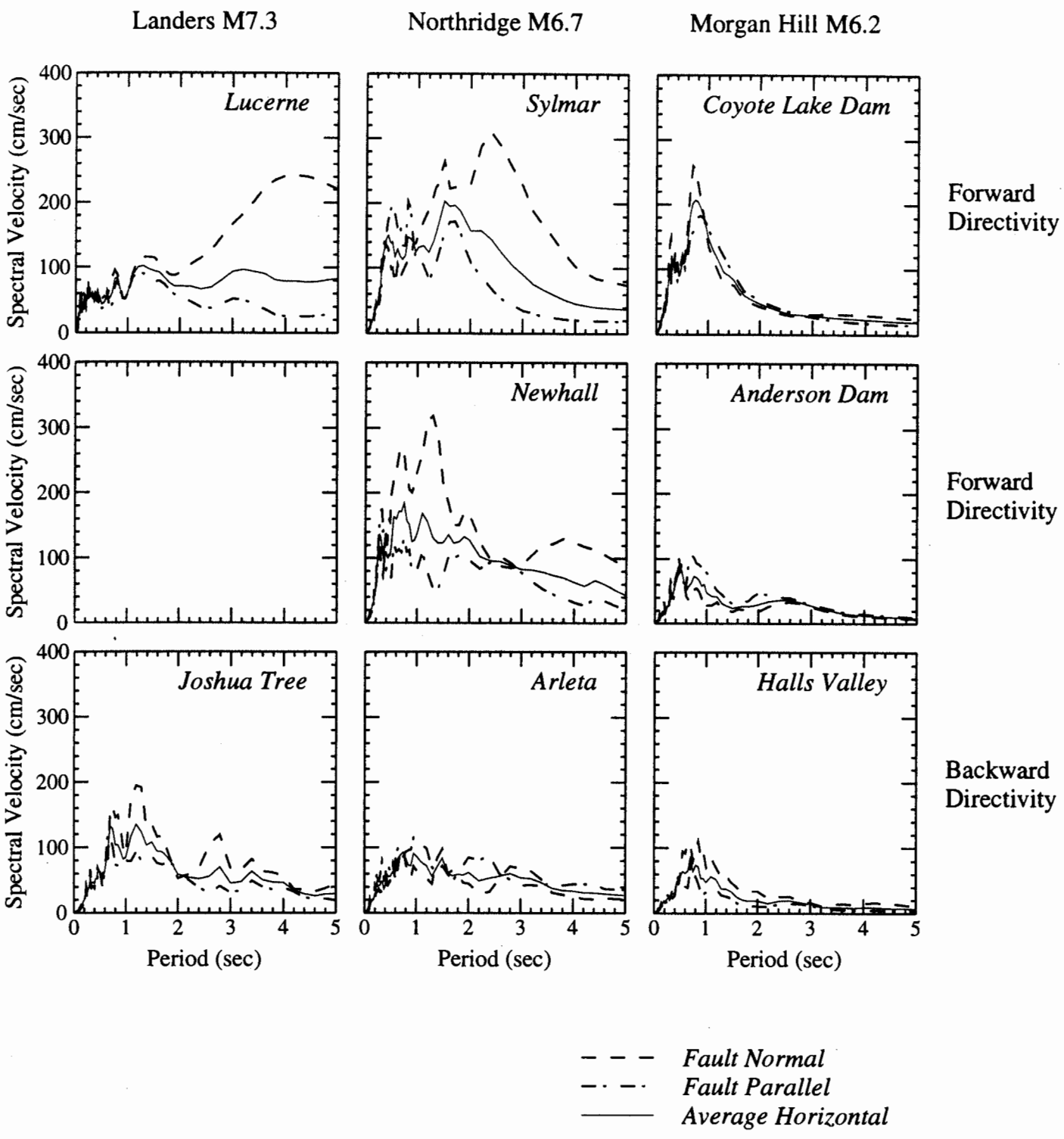

Figure 4. Response spectra of recorded time histories from 3 earthquakes showing dependence of spectrum on magnitude and directivity conditions.

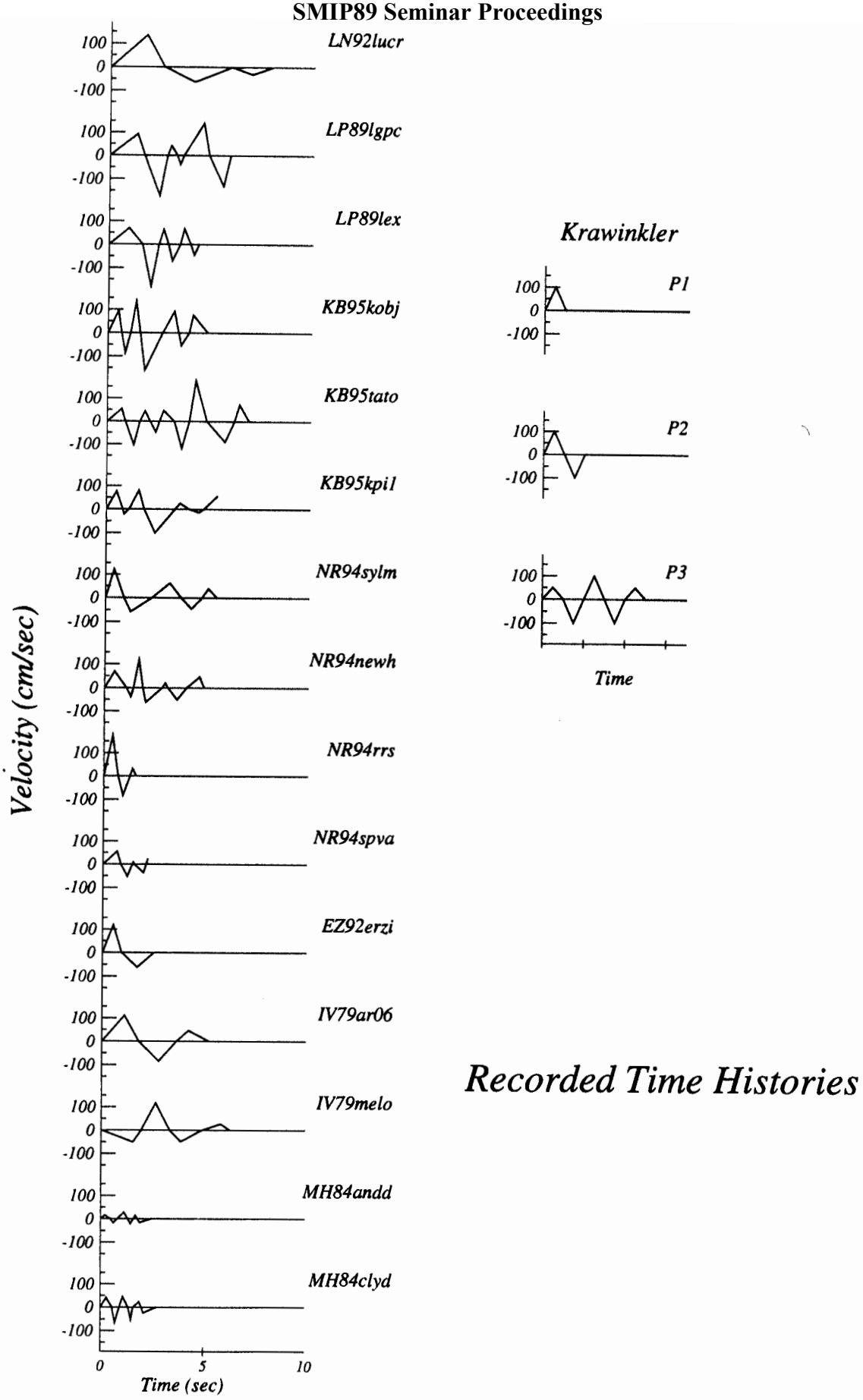

Figure 5. Left: Simplified representation of near fault velocity pulses in recorded ground motion. Right: Three representative pulses P1, P2 and P3 used in dynamic non-linear analyses by Krawinkler (1998).

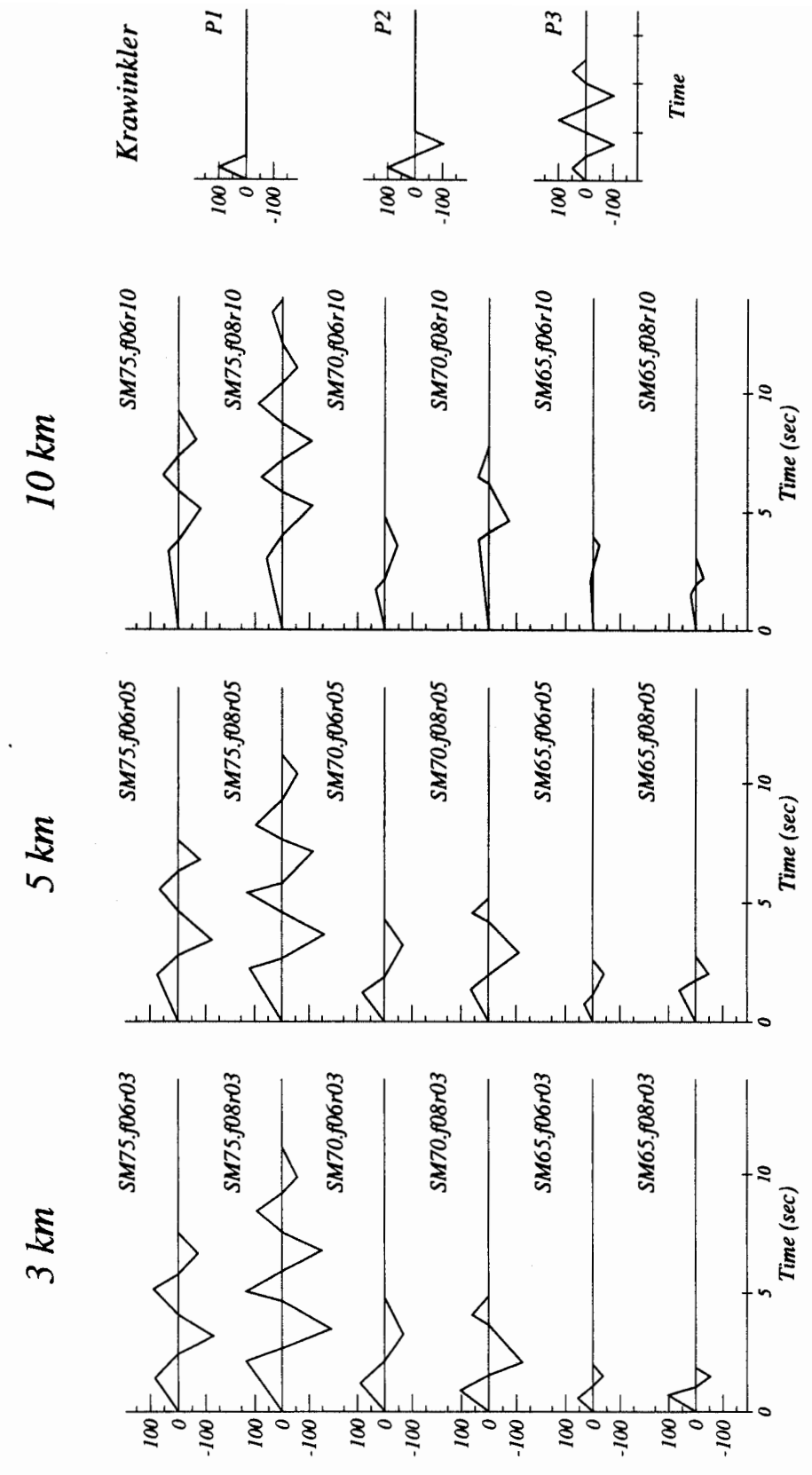

Figure 6. Left: Simplified representation of near fault velocity pulses in simulated ground motion. Right: Three representative pulses P1, P2 and P3 used in dynamic non-linear analyses by Krawinkler (1998).

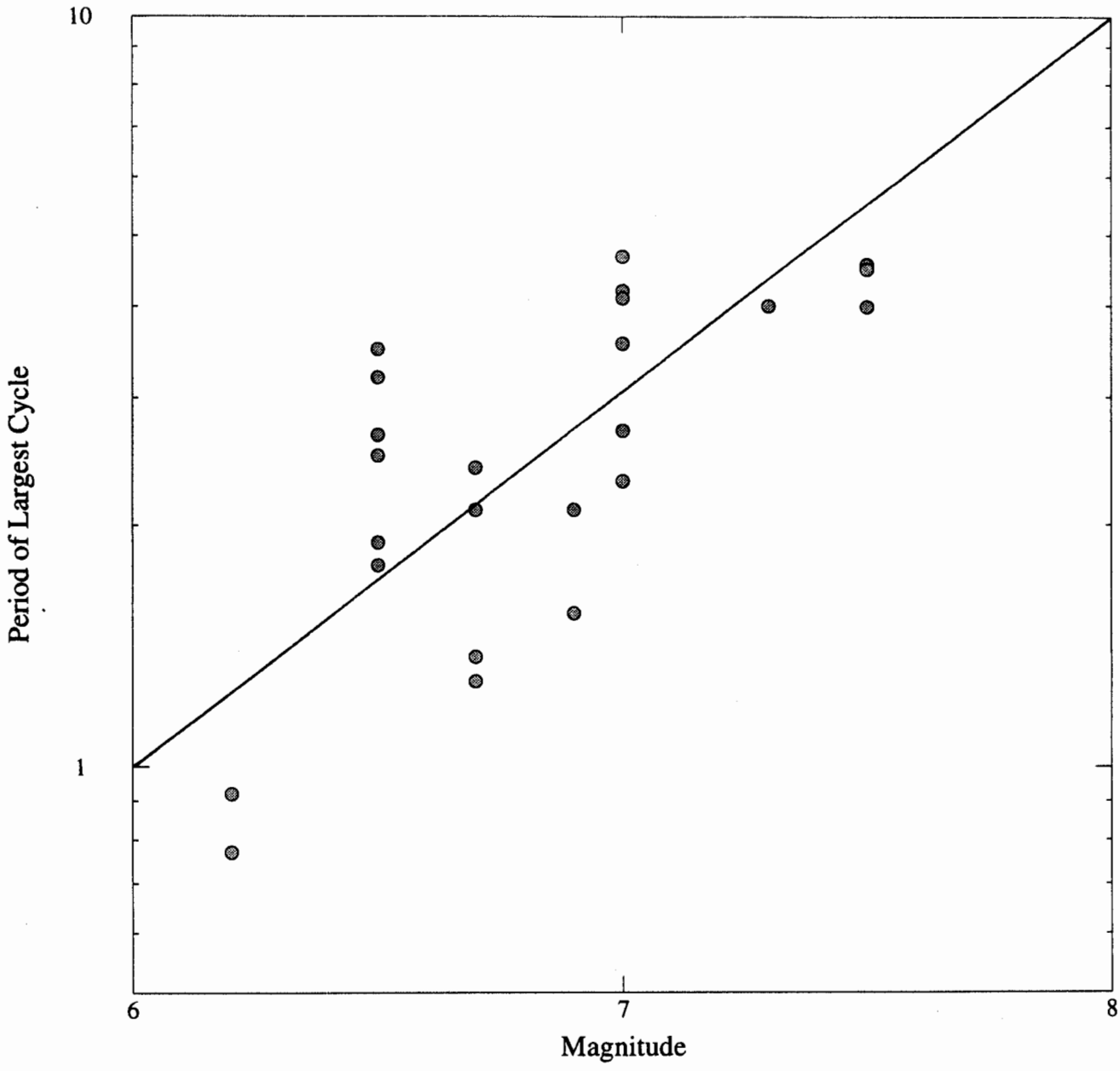

Figure 7. Relationship between the period of the largest cycle and magnitude.

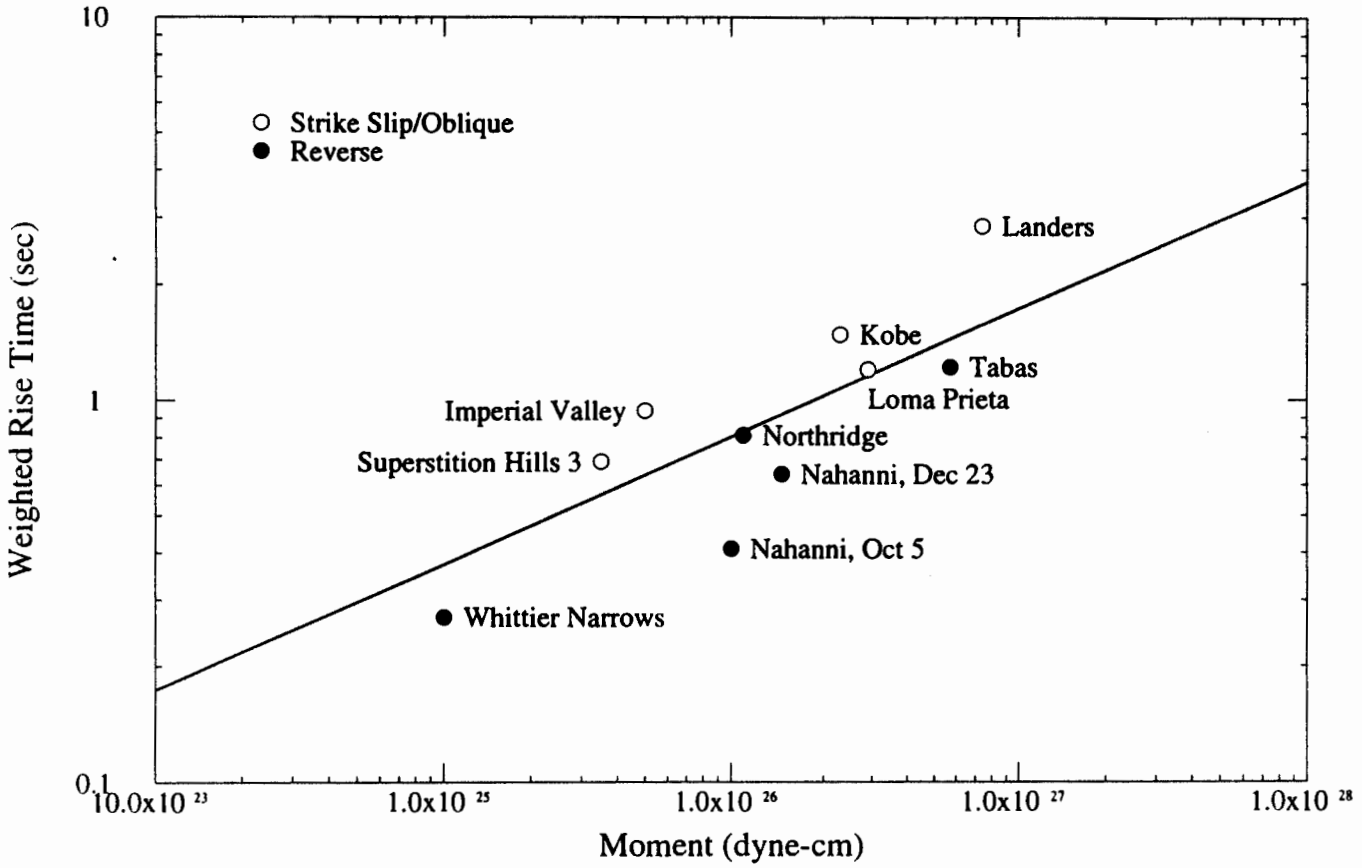

Figure 8. Relationship between rise time and seismic moment for crustal earthquakes. The rise times of reverse faulting earthquakes all fall below the self-similar relation derived from the data set as a whole, and those for strike-slip earthquakes fall above the relation.